Supporting Information

Synergistic Contribution of the Acidic Metal Oxide-Metal Couple and Solvent Environment in the Selective Hydrogenolysis of Glycerol: a Combined Experimental and Computational Study Using ReO_x-Ir as the Catalyst

Jithin John Varghese,[a 1] Liwei Cao,[a,b 1] Christopher Robertson,[a,b] Yanhui Yang,[a,c,d] Lynn F. Gladden,[a,b] Alexei A. Lapkin,[a,b*] Samir H. Mushrif[a,c,e*]*

[a] Cambridge Centre for Advanced Research and Education in Singapore (CARES) Ltd., Campus for Research Excellence and Technological Enterprise (CREATE), CREATE Tower, 1 CREATE Way, Singapore, 138602

[b] Department of Chemical Engineering and Biotechnology, University of Cambridge, Philippa Fawcett Drive, Cambridge CB3 0AS, U.K.

[c] *School of Chemical and Biomedical Engineering, Nanyang Technological University Singapore, 62 Nanyang Drive, Singapore, 637459*

[d] *School of Chemistry and Molecular Engineering, Nanjing Tech University, Nanjing, China*

[e] *Department of Chemical and Materials Engineering, University of Alberta, 9211 - 116 St. NW, Edmonton, Alberta, T6G 1H9, Canada*

Email: lfg1@cam.ac.uk (LFG), aal35@cam.ac.uk (AAL), mushrif@ualberta.ca (SHM)

[1] Both authors contributed equally to this work.

This document contains additional details regarding the experimental and computational methods, additional supporting results including Figures S1 to S18, Tables S1 and S2, and references.

S1. Experimental methods

S.1.1. Catalyst preparation

SiO_2 (6 nm pore size, 700 m^2g^{-1} ± 50 m^2g^{-1} surface area) supplied by Sigma-Aldrich Co. LLC was used as a support for the catalysts. The Ir catalyst was prepared by impregnating silica with an aqueous solution of H_2IrCl_6 (Sigma-Aldrich Co. LLC.), followed by drying at 373 K for 12 hours. The ReO_x catalyst was prepared by using NH_4ReO_4 (Sigma-Aldrich Co. LLC.) as a precursor. Both types of catalyst were calcined in air at 773 K for 3 hours after the drying procedure. Physical mixture of the Ir and ReO_x, where each of them was synthesized in the methods described earlier, constituted the third kind of catalyst and is designated as Ir + ReO_x. The ReO_x-Ir catalyst was prepared by sequential incipient wetness impregnation. SiO_2 was first impregnated with aqueous solution of H_2IrCl_6, followed by drying at 373 K for 12 hours and calcination at 773 K for 3 hours. Then rhenia was deposited on the Ir by the same procedure with an aqueous solution of NH_4ReO_4.

S1.2. Catalyst characterization

BET analysis was conducted with ASAP 2020 V3.04 H, and the samples were degassed at 423 K under vacuum for 2 h. The total pore volume was defined as the single-point pore volume at a relative pressure $p/p_0 = 0.95$. The X-ray powder diffraction (XRD) data was collected using Bruker D2 Phaser XRD with Cu K_α radiation. The X-ray patterns were measured at the 2θ range of 10-80° at 40 kV and 40 Ma. Both the as synthesized and H_2 pre-treated catalysts before the reaction

were analyzed. X-ray photoelectron spectroscopy (XPS) analysis of the samples was performed on a Kratos AXIS Ultra DLD surface analyzer using a monochromatic Al Ka radiation source at 15 kV (1486.71 eV). Here again, both the as synthesized and H_2 pre-treated catalysts before the reaction were analyzed. The pressure in the analysis chamber was around 7.1×10^{-5} Pa. The metal loadings of the Ir-Re based catalysts were determined by inductively coupled plasma optical emission spectroscopy (ICP-OES, Agilent 720) after dissolving in hydrofluoric acid (HF). The liquid phase after the reaction was also analyzed by inductively coupled plasma mass spectrometry (ICP-MS, Agilent 7700) for detecting the leaching of the catalyst components during the glycerol hydrogenolysis reaction process. To investigate the acidic nature of the catalysts, pyridine adsorption and Fourier transform infrared spectroscopy (FT-IR) was performed on the reduced catalysts. 20 mg of the reduced catalyst sample was first outgassed at 423 K for 2 h in vacuum (around 10^{-2} Pa), and then cooled down to 291 K for recording the background spectra. After adsorption of pyridine at 291 K, the sample was evacuated at 423 K for 1 h, and the FT-IR spectra of absorbed pyridine was recorded at 291 K.

S1.3. Catalytic reactions

Glycerol hydrogenolysis reactions were carried out in a stainless-steel reactor with Teflon liner (Parr 4950, controller 4843, Parr Instrument Company, USA). 100 mg of the catalyst was added to the Parr reactor together with an appropriate amount of water and heated at 473 K with 8 MPa H_2 for an hour for the catalyst reduction pre-treatment. After the pre-treatment, the reactor was cooled down with ice water and the hydrogen was removed and glycerol (Sigma-Aldrich Co. LLC., > 99.5%) was added into the reactor. The air residue inside the reactor was expelled by pressurizing and releasing hydrogen three times. In some cases, dilute sulfuric acid (Sigma-Aldrich Co. LLC., >98%) was used as a promoter. The standard condition for the reactions unless specified otherwise

were as follows: reaction temperature - 393 K, initial hydrogen pressure - 8 MPa, reaction time - 24 h, glycerol amount - 2 g, water amount - 8 g, H_2SO_4 (H^+/Ir= 1) - 1 mg and catalyst amount - 100 mg. The effect of different parameters on glycerol conversion and product selectivity were investigated by changing these appropriately. The resulting reaction mixture was analyzed by HPLC equipped with a multiple wavelength detector and a gas chromatograph-mass spectrometer (GC-MS) equipped with a flame ionization detector and a HP-5 capillary column. The used catalyst was collected by centrifugation, washed with de-ionized water three times and dried in air and calcined at 773 K for 3 h. A slight loss (<10% in weight) was observed during the recovery process and was compensated with fresh catalyst in each reuse experiment.

S2. Computational methods

S2.1. *Ab initio* molecular dynamics of aqueous glycerol

Ab initio molecular dynamics simulations of aqueous glycerol and aqueous glycerol with acid were performed implementing the Car-Parrinello molecular dynamics[1] scheme in the CPMD package[2]. One glycerol molecule with 108 water molecules in a cubic box of 15 Å per side was used to represent aqueous glycerol. The same system with one of the water molecules converted into a hydronium ion was used to represent the aqueous glycerol with acid. CPMD simulations with plane-wave pseudopotential implementation of Density Functional Theory (DFT)[3-4] were performed using the Perdew-Burke-Ernzerhof (PBE)[5] exchange correlation functional and norm conserving Troullier Martins[6] pseudopotential with a plane wave expansion cut off energy of 80 Rydberg (Ryd.) After optimizing the geometry of the systems, both the systems were thermalized at temperature of 363 K for 0.5 ps using a velocity rescale algorithm. The fictitious mass of the electronic system was fixed at 500 atomic units and the time step for integration of equations of motion was fixed at 4 atomic units (0.0968 fs) in these simulations. The systems were further

equilibrated for 4 ps where the temperature was maintained at 363 K with the Nose-Hoover[7-8] chain thermostat. The frequency of the ionic thermostat was set at 3400 cm^{-1} and that of the electronic thermostat at 12000 cm^{-1}. The trajectories were visualized and analyzed in Visual Molecular Dynamics (VMD) package[9].

S2.2. Classical molecular dynamics simulations

Classical molecular dynamics simulations of 20% aqueous glycerol solutions were also performed at 298 K to investigate the solvation of glycerol in water. The OPLS-AA force field parameters[10] were used in the simulations of aqueous glycerol and the simulations were performed using the GROMACS package. Since typical classical molecular dynamics simulations cannot treat protons or hydronium ions, one Na^+ ion was added to one of the simulation systems containing 55 glycerol molecules and 1185 water molecules contained in a cubic box of 35 Å side, to mimic the effect of an H^+. A chloride ion was also added to this simulation system to neutralize the charge. The other system contained the same number of glycerol molecules and 1187 water molecules, without the Na^+ and Cl^- ions in the same box. These two systems were equilibrated at 298 K for 100 ps using a velocity rescale algorithm. This was followed by MD simulations in the NPT ensemble to obtain the density corresponding to 20% glycerol solution for 200 ps. Subsequently, MD simulations in the NVT ensemble were performed using the Nosé–Hoover thermostat[7-8] for 10 ns. In all the MD simulations, all bonds were constrained using the LINCS algorithm[11] and the MD time-step was fixed at 2 fs.

S3. Results

S3.1. Catalyst Characterization

The XRD patterns for the ReO_x-Ir catalyst, before and after reduction, are shown in Figure 2a of the article. The diffraction peak at 2θ of around 29° is attributed to amorphous silica. The diffraction peaks corresponding to IrO_2 (101) at 2θ = 34.7°, IrO_2 (200) at 2θ = 40.1°, IrO_2 (211) at 2θ = 54.0°, IrO_2 (112) at 2θ = 66.1° (PDF #43-1019) were observed in the as synthesized catalysts. The peaks due to ReO_x species were not detected, suggesting their high dispersion. A diffusive diffraction peak corresponding to Ir (111) metallic particle at 2θ = 40.7° (PDF #46-1044), was observed for the catalyst sample after its pre-treatment in hydrogen and was accompanied by the disappearance of diffraction peaks corresponding to IrO_2.

Table S1. Summary of Brønsted acid and Lewis acid sites on the different catalysts as identified by pyridine adsorption and FT-IR analysis based on Ref.12[12]

Catalyst	Brønsted acid sites (cm^{-1})			Lewis acid sites (cm^{-1})	
	1635	1540	1490	1490	1457
Ir	×	×	×	×	×
ReO_x	×	√	√	√	√
Ir + ReO_x	√	√	√	√	√
ReO_x-Ir	√	√	√	√	√

S3.2. Formation of Re-OH/ Re-OH-Re species on ReO_x clusters in ReO_x-Ir catalysts and their characterization

The reduction pre-treatment of the ReO_x-Ir catalyst is believed to be one of the reasons for the Brønsted acidity of the catalyst, as it introduces Re-OH species.[13] Higher temperatures during reduction pre-treatment are believed to generate higher acidity.[14] Hence, hydrogenation of Re=O

and Re-O-Re on Re_3O_6/Ir(111) by active hydrogen (dissociatively adsorbed) on the Ir(111) surface was investigated using DFT calculations and the results are shown Figure S1. Activation barriers were calculated only for the hydrogenation steps as the diffusion of hydrogen on the Ir surface is assumed to have barriers lower than hydrogenation steps. Direct hydrogenation of the Re=O (blue curve in Figure S1) has a high activation barrier of 177.6 kJ mol^{-1} from the intermediate represented by 2, while the barrier for the subsequent hydrogenation of Re-O-Re from the intermediate represented by 4 is 62.5 kJ mol^{-1}.

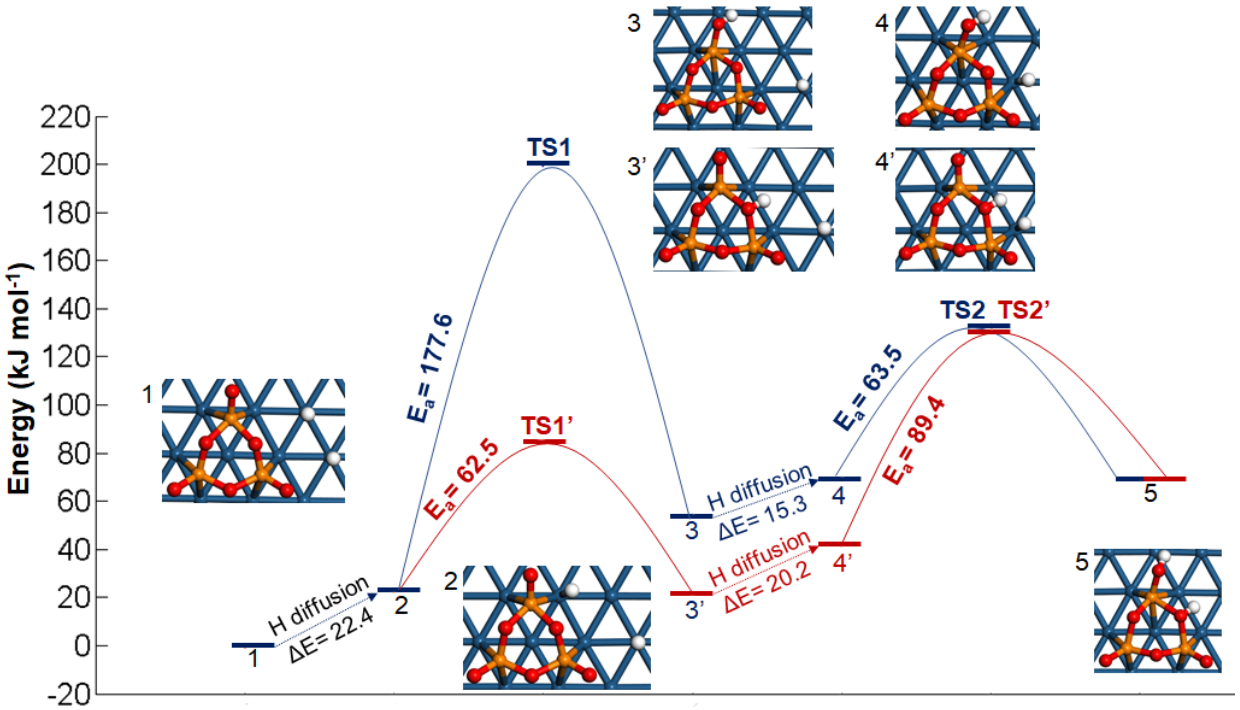

Figure S1 Pathways for hydrogenation of ReO_x on Re_3O_6/Ir(111) by dissociatively adsorbed hydrogen on the Ir(111) surface. Color code is the same as in Figure 3 of the article.

However, the barrier for the hydrogenation of Re=O is significantly lower at 89.4 kJ mol^{-1} when it is preceded by the hydrogenation of Re-O-Re (intermediates are denoted by the 3' and 4') as depicted by the red curve in Figure S1. In both these routes, each hydrogenation step has a positive reaction energy. Sequential hydrogenation of the Re_3O_6 cluster along the pathway shown in red

color in Figure S1, results in the formation of Re-OH and Re-OH-Re with an overall activation barrier of 131.2 kJ mol^{-1}, suggesting the likelihood of formation of these species during reduction pre-treatment.

The other possible reason for the acidity of the ReO_x-Ir catalyst is believed to be the dissociation of water on the Re site which also leads to the formation of Re-OH.[15] Dissociation of a water molecule on an Re_3O_5 cluster on Ir(111) was investigated using DFT calculations and the results are shown in Figure S2. The dissociation of water to form Re-OH and H has a relatively high activation barrier of 113.8 kJ mol^{-1}. However, dissociation of water assisted by the hydrogen abstraction by the Re-O-Re, forming Re-OH and Re-OH-Re has a significantly lower activation barrier of 50.8 kJ mol^{-1}.

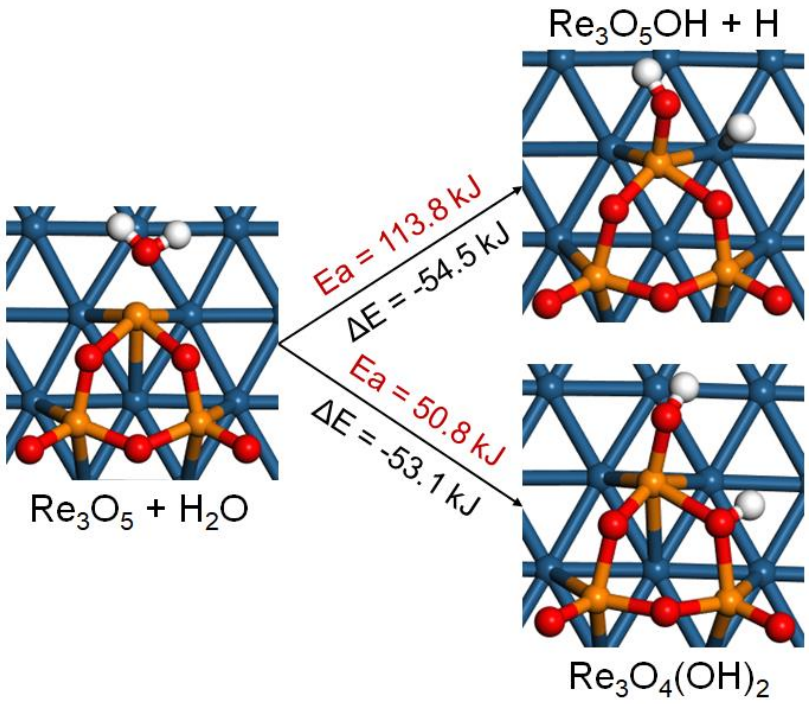

Figure S2 Dissociation of water at Re sites on ReO_x-Ir catalyst forming Re-OH + H and Re-OH + Re-OH-Re. Color code is the same as in Figure 3 of the article.

Both hydrogenation (hydrogen spillover) and dissociation of water are possible pathways for the formation of different kinds of hydroxyls (Re-OH and Re-OH-Re) on the ReO_x clusters, including the formation of vicinal hydroxyls on the same cluster. Since the hydroxyls can form under experimental conditions and they are expected to be Brønsted acidic, computational investigation of pyridine-H (pyridinium) deriving its H from Re-OH and Re-OH-Re species in $Re_3O_6H_3$ was performed. Vibrational analysis of the normal modes of pyridine-H yielded modes with frequency of 1537 cm^{-1} near the Re-OH species and 1541 cm^{-1} near the Re-OH-Re species. These modes represent the in-plane bending of the pyridine ring which is characteristic of a pyridinium ion formed by interaction with a Brønsted acid site.[16] Since these frequencies match those obtained from the FT-IR analysis of pyridine adsorption on the ReO_x-Ir catalyst at Brønsted acid sites (Figure 2e and Table S1 of the Supporting Information), Re-OH and Re-OH-Re species are ascertained to be the Brønsted acid sites.

S3.3. Glycerol conversion as a function of glycerol concentration

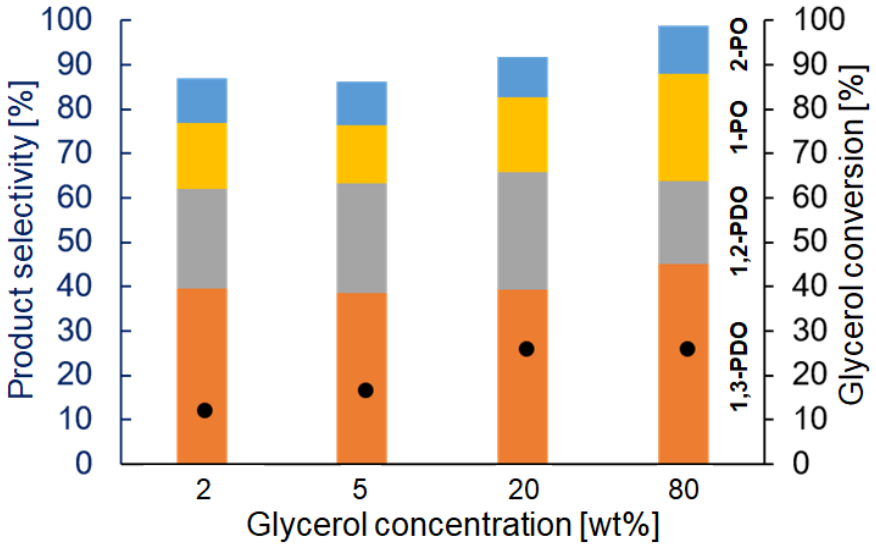

Figure S3 Variations in the conversion of glycerol and product selectivity during hydrogenolysis of glycerol on the ReO_x-Ir catalyst at different initial glycerol concentrations without sulfuric acid.

S3.4. Effect of sulfuric acid on the glycerol-water interaction and formation of free hydronium ions from Brønsted acidic ReO_x clusters

Computational investigation of solvation of solutes/reactants in a solvent/solvent mixture can be done using two broad approaches: 1) implicit solvation, and 2) explicit solvation. The implicit solvation approach is a mean field approximation where the solvent perturbation is added to the solute/substrate Hamiltonian as homogeneous dielectric continuum. This method is not suitable for the investigation of solvation of glycerol due to the extensive intermolecular hydrogen bonding network associated with its aqueous solution. Hence the solvation of glycerol must be investigated using explicit solvent molecules considered in the simulation system. Due to the need for configurational sampling over time at finite temperatures, molecular dynamics simulations are ideal to investigate solvation of polyols like glycerol in water. Hence, the interaction of glycerol with water was studied using a combination of *ab initio* molecular dynamics (AIMD) simulations and DFT calculations. Sulfuric acid in water readily forms hydronium ions and hence, the acid containing sample was modelled with one hydronium ion in the system.

Ab initio molecular dynamics simulations of aqueous glycerol in the absence and presence of a hydronium ion were performed as described in section S2.1 of the supporting information. The configurations of the hydronium ion containing (acidic) glycerol were extracted from the MD trajectory at regular intervals of 0.4 ps. Each of these configurations were further optimized using the VASP code.[17] The optimized configuration at the end of 4 ps of MD simulations is shown in Figure S4a. For each of the extracted configurations, single point energy calculations were performed without further geometry optimization with 1) only the hydronium ion and water molecules (by removing the glycerol) and, 2) only glycerol (by removing the water molecules and the hydronium ion). Figures S4b and c represent the aqueous hydronium ion containing system

and glycerol respectively, as derived from the configuration shown in Figure S4a. For each of the configurations extracted from the MD trajectory, the interaction energy of glycerol with the acidic aqueous medium was calculated as the difference in energy of the complete system and the decomposed systems as

$$E_{(a)}-\{E_{(b)} + E_{(c)}\} \quad (1)$$

The same process was repeated for each of the configurations extracted from the MD trajectory of the aqueous glycerol system (without hydronium ion). Figure S4d represents the configuration of the aqueous glycerol system at the end of 4 ps of MD simulations. The configurations of water molecules alone and glycerol alone as obtained from the structure in Figure S4d are shown in Figures S4e and f respectively. For each of the configurations extracted from the MD trajectory, the interaction energy of glycerol with water was calculated as the difference in energy of the complete system and the decomposed systems as

$$E_{(d)}- \{E_{(e)} + E_{(f)}\} \quad (2)$$

The average interaction energy of glycerol with acidic water was calculated to be 350.6 kJ mol^{-1} while it was 288.1 kJ mol^{-1} for the pure aqueous system. The larger negative value of interaction strength for the system containing the hydronium ion compared to the pure aqueous system suggests that the glycerol-water interaction is significantly enhanced in the presence of hydronium ions.

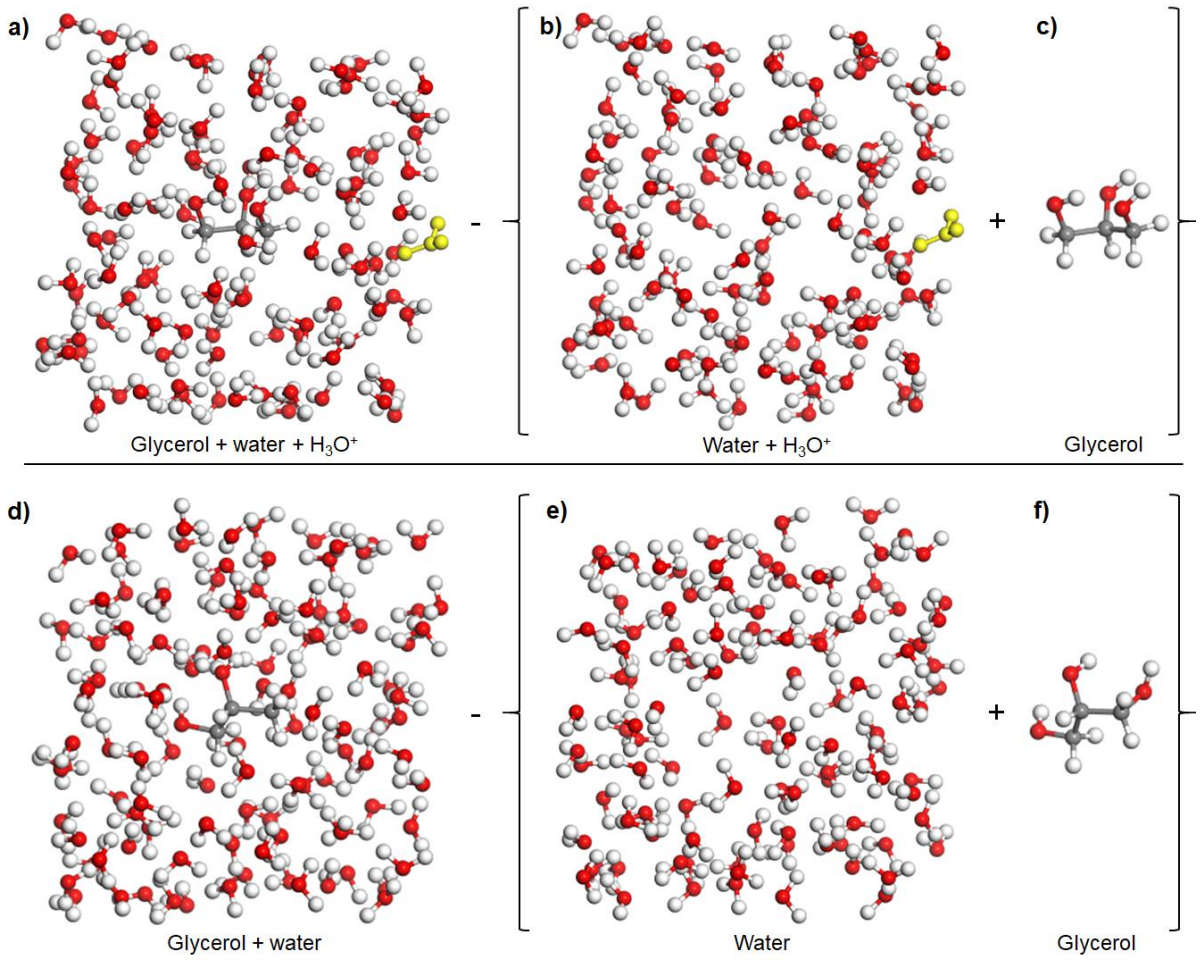

Figure S4 DFT optimized structures of aqueous glycerol as obtained from *ab initio* molecular dynamics simulations in the presence of **a)** a hydronium ion and water molecules and **d)** only water. The hydronium ion is highlighted in yellow. The systems comprising **b)** the hydronium ion and water (without glycerol), **c)** glycerol; both in the same configurations as in part **a)** are also shown. Also shown are systems comprising **e)** water molecules (without glycerol) and **f)** glycerol; both in the same configuration as in part **d)**. Color code is the same as in Figure 8 of the article.

The difference between the interaction of glycerol with the acidic aqueous medium and pure water is believed to be due to the difference in the hydrogen bonding of glycerol with water in the two cases. To investigate this further, classical molecular dynamics simulations of glycerol-water systems were performed. The simulation systems and the methods employed are described in

section S2.2 of the Supporting information. One of the simulation systems mimicked the acid containing glycerol, containing Na^+ and Cl^- ions, while the other was purely aqueous glycerol. The life time of hydrogen bonds between glycerol and water is a direct indication of the strength of interaction of glycerol with water. The glycerol-water hydrogen bond lifetimes were determined for both the systems by averaging over all the autocorrelation existence functions of the hydrogen bonds as per the theory of Luzar and Chandler[18]. The obtained hydrogen bond lifetime for the aqueous glycerol system was 2.37 ps while that of the aqueous glycerol containing Na^+ ion was 3.17 ps. The lifetime of hydrogen bonding between glycerol and water in the system containing Na^+ ion is higher than that of the pure aqueous system, showing that the interaction of glycerol with water is stronger for such systems. The same trend was obtained earlier where we combined AIMD simulations with DFT calculations and found the interaction of glycerol with water in the presence of hydronium ion to be stronger. This hydrogen bonding analysis provides further support to this claim.

To understand the deprotonation behavior of the Brønsted acidic Re-OH-Re on ReO_x clusters to form free hydronium ions in aqueous media, DFT simulations of the deprotonation of Re-OH-Re, forming a hydrated hydronium ion were performed, both in the presence of an additional hydrated hydronium ion complex and without the hydronium ion (only water molecules). Figure S5a shows the $Re_3O_6H_3$/Ir(111) catalyst containing the Re-OH-Re species next to a hydrated hydronium ion complex comprising H_3O^+-H_2O-[12] (twelve water molecules) whose initial configuration was obtained from the *ab initio* molecular dynamics simulation described in S2.1 of the Supporting Information. The H_3O^+-H_2O-$_{12}$ complex comprises a hydronium ion surrounded by four immediate water neighbors (H_3O^+-H_2O-$_4$) and an additional eight water molecules which can stabilize another hydronium ion resulting from the deprotonation of the Brønsted acidic Re-OH-Re species. The

number of water molecules chosen also ensures that the resulting two hydronium ions do no interact with each other directly. When the hydronium ion described earlier is replaced by a water molecule, the system comprising $Re_3O_6H_3$/Ir(111) catalyst with thirteen water molecules, as shown in Figure S5c is formed.

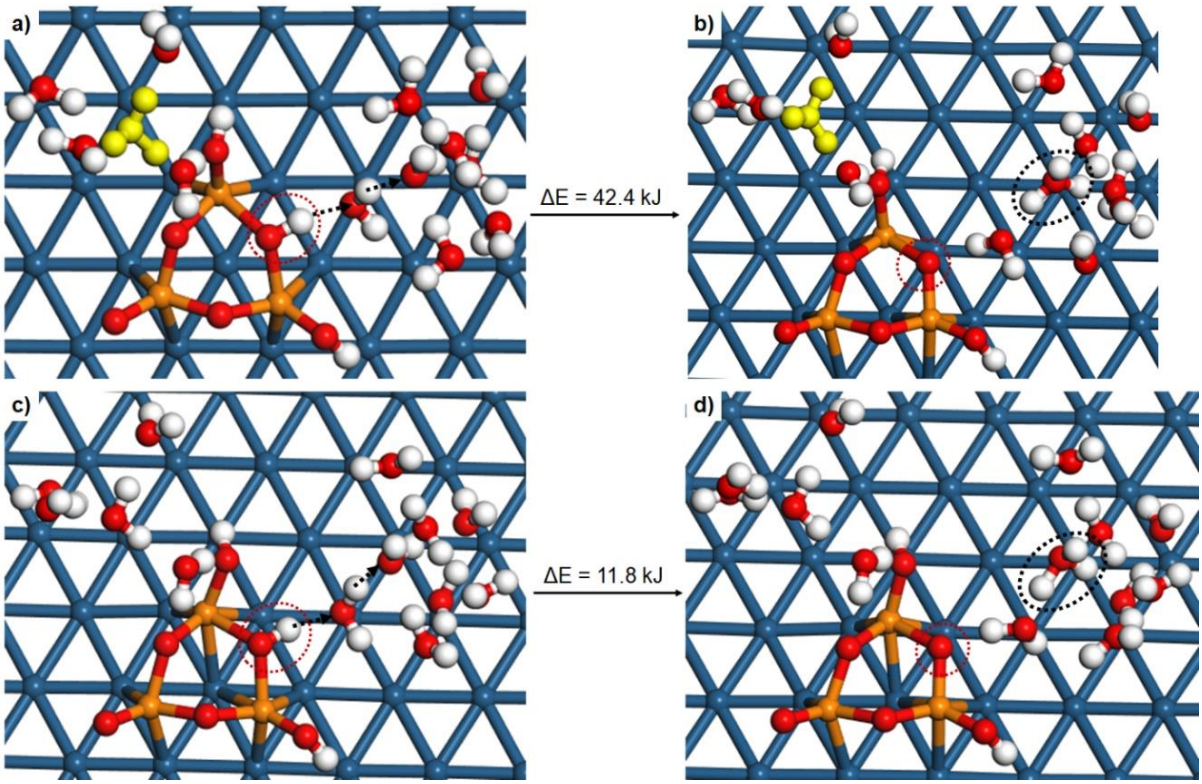

Figure S5 Deprotonation of Re-OH-Re species on $Re_3O_6H_3$/Ir(111) catalyst and formation of a hydrated hydronium ion cluster in the presence and absence of an additional hydronium ion. Initial configuration $Re_3O_6H_3$/Ir(111) catalyst in the presence of **a)** hydrated hydronium ion cluster represented by H_3O^+-H_2O-$_{12}$ (the hydronium ion is highlighted in yellow), and **c)** thirteen water molecules (no hydronium ion). The final configuration corresponding to the deprotonated $Re_3O_6H_2$/Ir(111) catalyst with **b)** two hydronium ions, and **d)** one hydronium ion. The newly formed hydronium ion is shown in dotted circle in each of these cases. The color code is the same as in Figure 3 of the article.

The deprotonation of $Re_3O_6H_3$ in both these systems resulted in a hydrated hydronium ion which is highlighted with the black dotted circles in Figures S5b and d. The reaction energy for the deprotonation of Re-OH-Re to form the hydrated hydronium ion in the presence of the additional hydronium ion was calculated to be 62.4 kJ mol^{-1} while that in the absence of the hydronium ion (c to d) was calculated to be 11.8 kJ mol^{-1}. Although both reaction energies are positive, the deprotonation in the presence of a hydronium ion is less favorable than in the absence of one (in pure aqueous medium). This suggests that the deprotonation of the Re-OH-Re species on ReO_x clusters to form free hydronium ions in the liquid medium is less favorable in the presence of added sulfuric acid, implying that these sites become available for the protonation-dehydration mechanism described in section 3.4.2 of the article.

S3.5. Dissociative adsorption of glycerol and decrease in adsorption energy during multiple glycerol adsorption on ReO_x-Ir catalyst

The dissociative adsorption of glycerol on the $Re_3O_6H_2$/Ir(111) catalyst in different configurations are shown in Figure 8 of the article and the dissociative adsorption energy was calculated as

$$E\ (H_2O\text{-}Re_3O_5H/Ir(111)\text{-}OCH_2\text{-}CHOH\text{-}CH_2OH) - \{E\ (Re_3O_6H_2/Ir(111)) + E\ (OHCH_2\text{-}CHOH\text{-}CH_2OH)_{gas}\} \quad (3)$$

To understand the effect of sulfuric acid on the interaction of glycerol with the ReO_x-Ir catalyst, dissociative adsorption of glycerol on $Re_3O_6H_2$/Ir(111) was simulated in the presence and absence of a hydronium ion-water complex. A hydrated hydronium ion cluster represented by H_3O^+-H_2O-8 as obtained from the *ab initio* molecular dynamics simulation (refer S2.1 for details) was used. This complex was placed suitably next to the hydroxyls of glycerol to facilitate the hydrogen

bonding interactions. The optimized structure, with the H_3O^+ species encircled, is shown in Figure S6a. The hydronium ion was replaced by a water molecule, with the remaining water molecules kept as it is (total of 9 water molecules), to simulate the dissociative attachment in the absence of acid. The optimized structure is shown in Figure S6c. The dissociative attachment of glycerol forming a primary propoxide and a molecule of water (Figure S6b), in the presence of the hydronium ion cluster, was calculated to have a reaction energy of -82.6 kJ mol^{-1} while the dissociative attachment in the absence of the hydronium ion (only water molecules, Figure S6d) was calculated to have a reaction energy of -64.1 kJ mol^{-1}. The dissociative attachment of glycerol is more favorable by 18 kJ mol^{-1} in the presence of the hydronium ion cluster suggesting a higher propensity for dissociative attachment of glycerol in the presence of the acid.

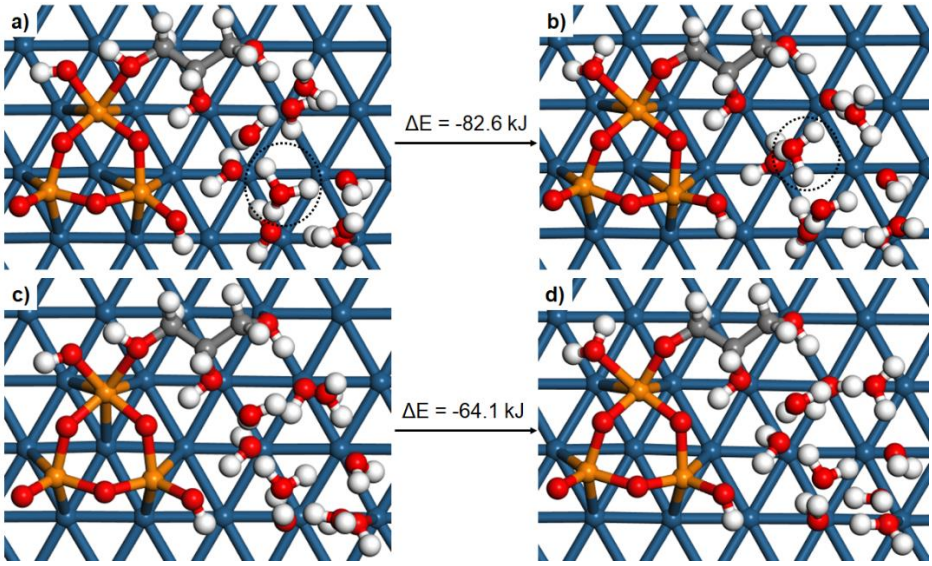

Figure S6 Initial configuration for the dissociative attachment of glycerol on the $Re_3O_6H_2$-Ir(111) catalyst and formation of a primary propoxide in the presence of **a)** hydrated hydronium ion cluster represented by H_3O^+-H_2O-$_8$ and **c)** nine water molecules. The corresponding final configurations of dissociatively adsorbed glycerol are shown in b) and d) respectively. Color code is the same as in Figure 8 of the article.

The dissociative adsorption of two glycerol molecules on the $Re_3O_6H_2$-Ir(111) catalyst in two different configurations are shown in Figure 8 of the article. The adsorption energy of two glycerol molecules adsorbing on the catalyst was calculated as

$$E\ (2H_2O\text{-}Re_3O_4/Ir(111)\text{-}(OCH_2\text{-}CHOH\text{-}CH_2OH)_2) - \{E\ (Re_3O_6H_2/Ir(111)) + 2 * E\ (OHCH_2\text{-}CHOH\text{-}CH_2OH)_{gas}\} \quad (4)$$

The adsorption energy of the second glycerol molecule attaching to the $Re_3O_6H_2$ cluster containing one adsorbed glycerol was calculated as

$$[E\ (2H_2O\text{-}Re_3O_4/Ir(111)\text{-}(OCH_2\text{-}CHOH\text{-}CH_2OH)_2) - \{E\ (H_2O\text{-}Re_3O_5H/Ir(111)\text{-}OCH_2\text{-}CHOH\text{-}CH_2OH) + E\ (OHCH_2\text{-}CHOH\text{-}CH_2OH)_{gas}\} \quad (5)$$

The difference in the adsorption energy of the second glycerol molecule adsorbing on the $Re_3O_6H_2$ cluster containing one adsorbed glycerol calculated with respect to the first dissociative attachment, calculated as

(5) – (3)

was found to be around 22 kJ mol^{-1}. This means that the dissociative attachment of the second glycerol molecule is less favorable by 22 kJ mol^{-1} compared to the first dissociative attachment. A similar value is obtained for the dissociative attachment via the secondary hydroxyl. This implies that dissociative adsorption of multiple glycerol molecules on the same ReO_x cluster, although has a negative reaction energy, becomes less favorable compared to single molecule adsorption. Hence, at low concentrations of glycerol near the catalyst, the saturation adsorption of glycerol on individual ReO_x clusters may not be likely. Saturation of individual ReO_x clusters may be possible at higher concentration of glycerol, although with a lowering of the average binding strength of glycerol.

S3.6. Energy profiles and transition states for glycerol hydrogenolysis on $Re_3O_6H_2$-Ir(111) catalyst by direct dehydroxylation mechanism

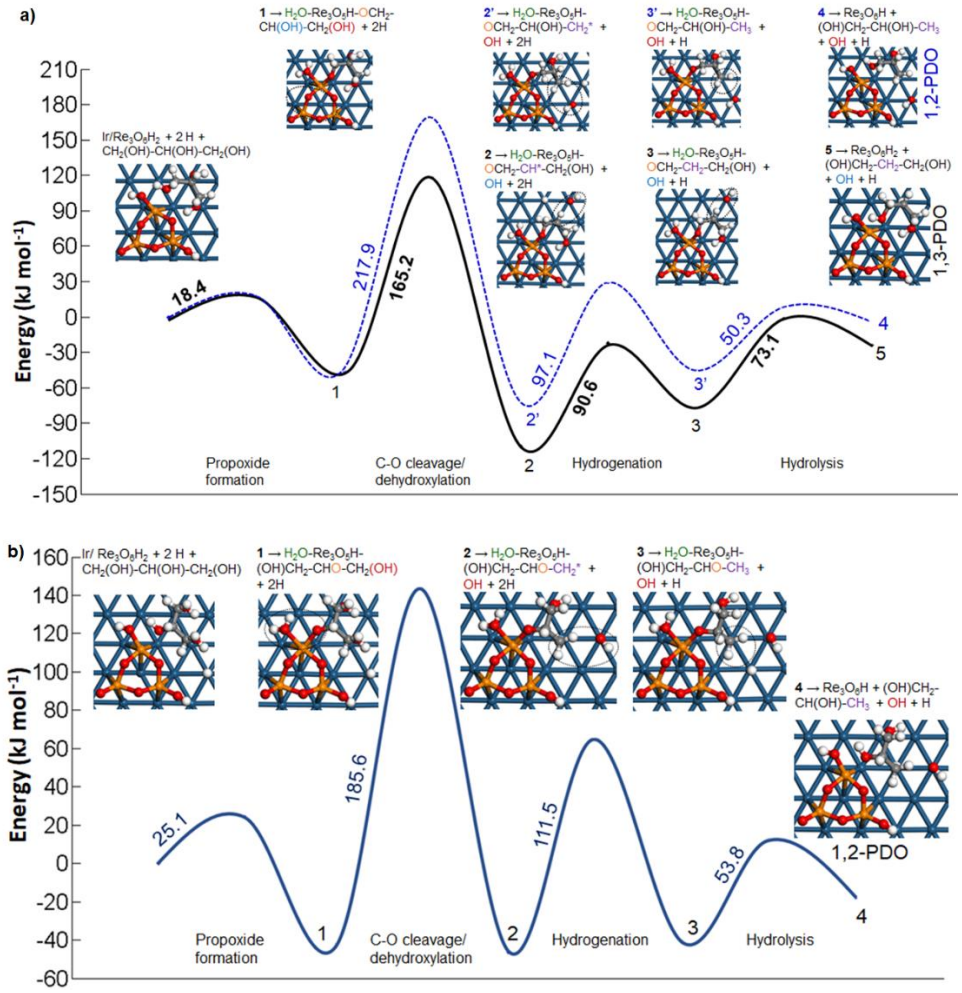

Figure S7 Energy profiles for the hydrogenolysis of glycerol on $Re_3O_6H_2$-Ir(111) catalyst initiated by the dissociative attachment of glycerol on the $Re_3O_6H_2$ cluster as **a)** a primary propoxide and **b)** as a secondary propoxide. In part a), the two possible products resulting from the elimination of the secondary hydroxyl (black solid line) or the primary hydroxyl (blue dotted line) are shown. The activation energy barrier associated with each step is indicated in the figure

with representative images and description of the intermediates/products. Color code is the same as in Figure 8 of the article.

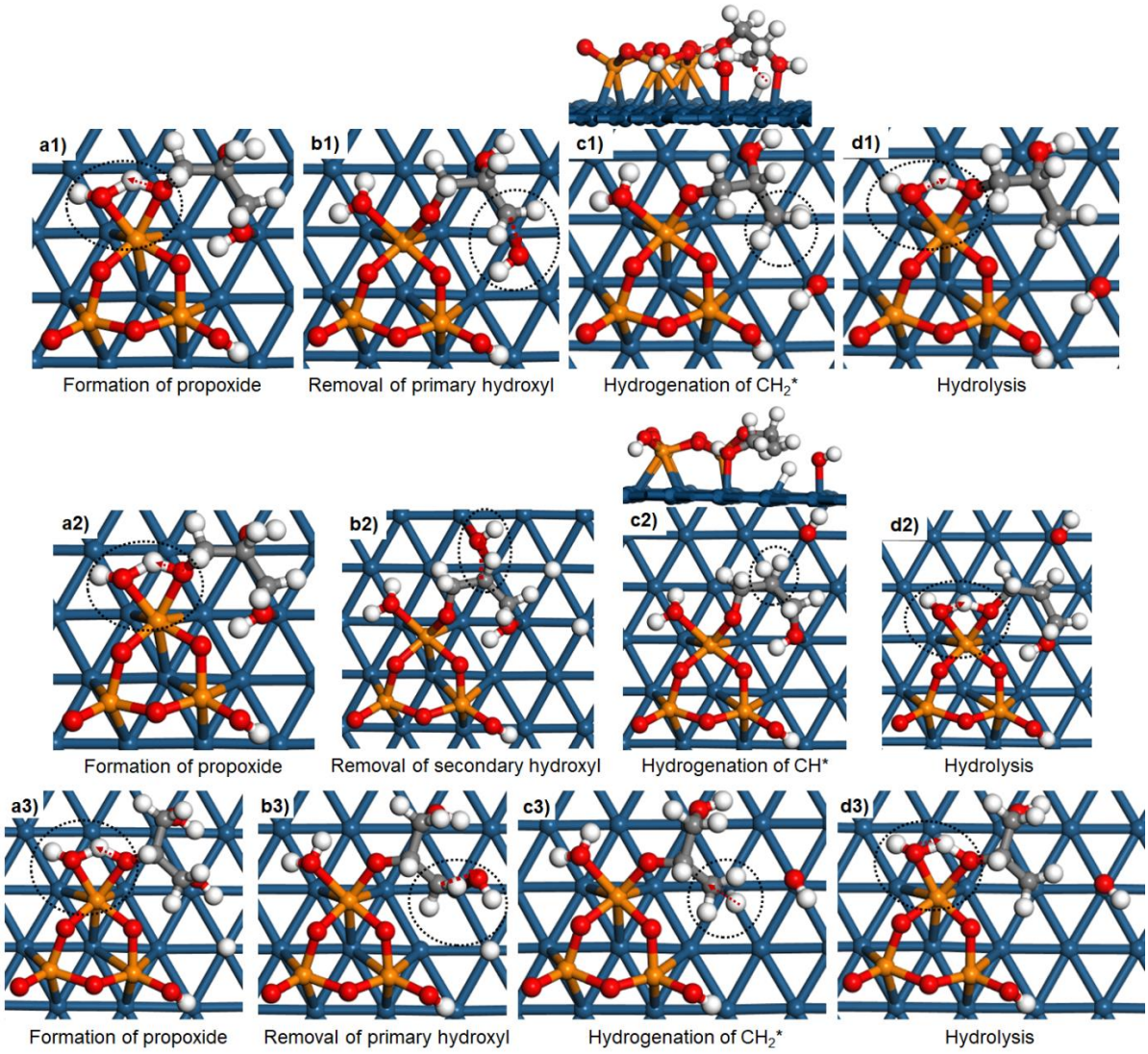

Figure S8 Transition states (TSs) for the elementary steps in hydrogenolysis of glycerol on $Re_3O_6H_2$-Ir(111) catalyst. The top panel (a1-d1) shows the pathway involving the removal of the primary hydroxyl to form 1,2-PDO and the middle panel (a2-d2) shows the removal of the secondary hydroxyl to form 1,3-PDO. Both these pathways are initiated by the dissociative attachment of glycerol through its primary hydroxyl as shown in Figure S7a. The bottom panel (a3-d3) shows the TSs for the elimination of the primary hydroxyl to form 1,2-PDO, following the

dissociative attachment through its secondary hydroxyl as shown in Figure S7b. Color code is same as in Figure 8 of the article.

S3.7. Energy profiles and transition states for glycerol hydrogenolysis on $Re_3O_6H_3$-Ir(111) catalyst by protonation-dehydration mechanism

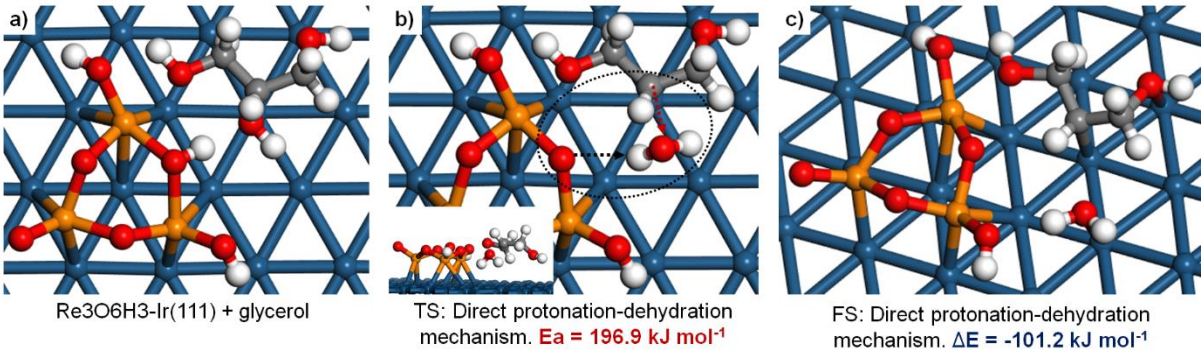

Figure S9 Direct protonation-dehydration of glycerol on $Re_3O_6H_3$-Ir(111) catalyst surface showing **a)** molecularly adsorbed (physisorbed) glycerol on the catalyst, **b)** transition state (TS) for the protonation-dehydration step and **c)** the final state (FS) with the CH* of glycerol and eliminated H_2O interacting with the Ir(111) surface. Color code is same as in Figure 8 of the article.

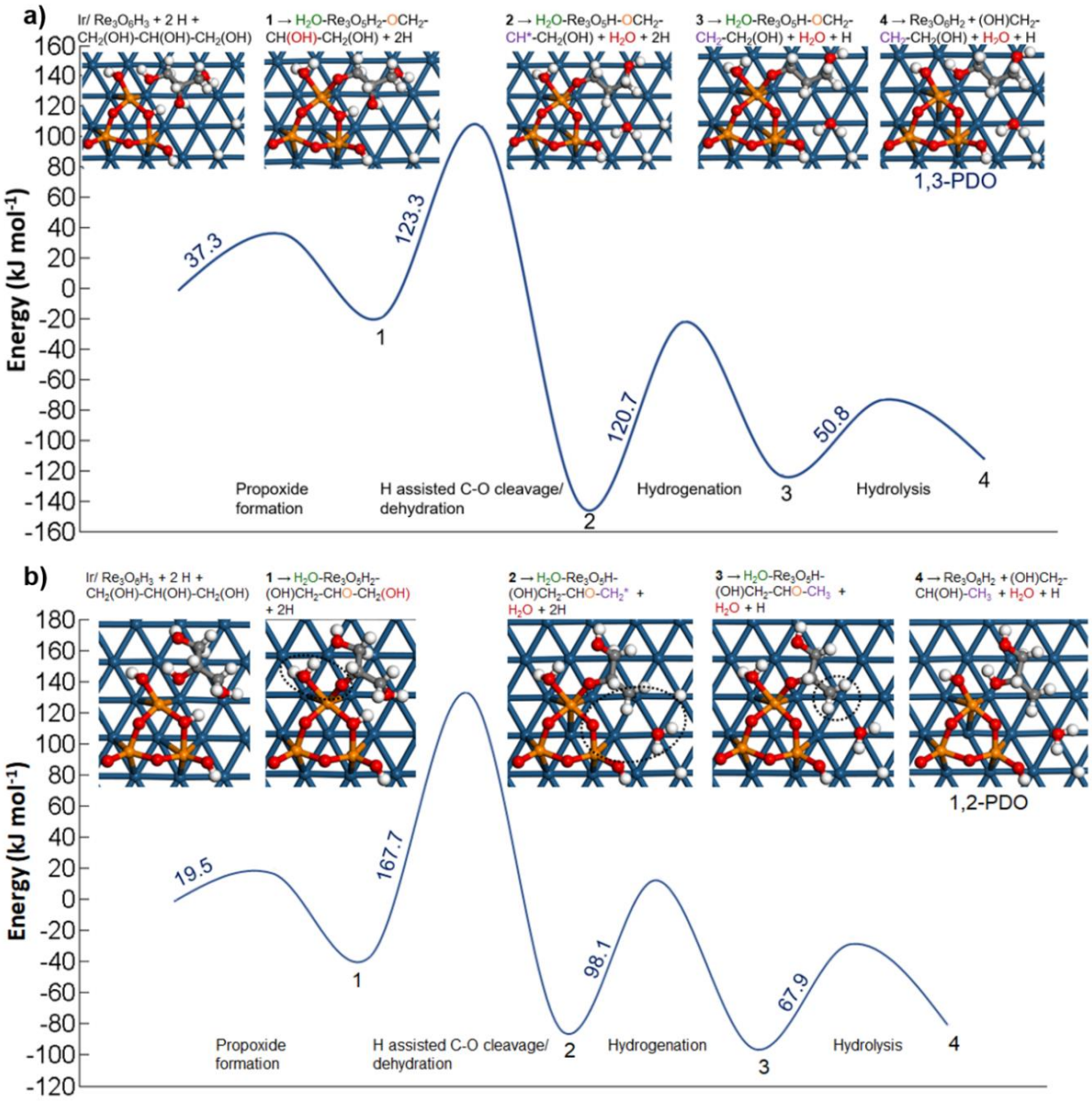

Figure S10 Energy profiles for the hydrogenolysis of glycerol on $Re_3O_6H_3$ cluster on Ir(111) surface via the protonation-dehydration mechanism initiated by the attachment of glycerol as **a)** a primary propoxide and **b)** a secondary propoxide. The activation energy barrier associated with each step is indicated in the figure with representative images and description of the intermediates/product. Color scheme for molecular structures is the same as in Figure 8 of the article.

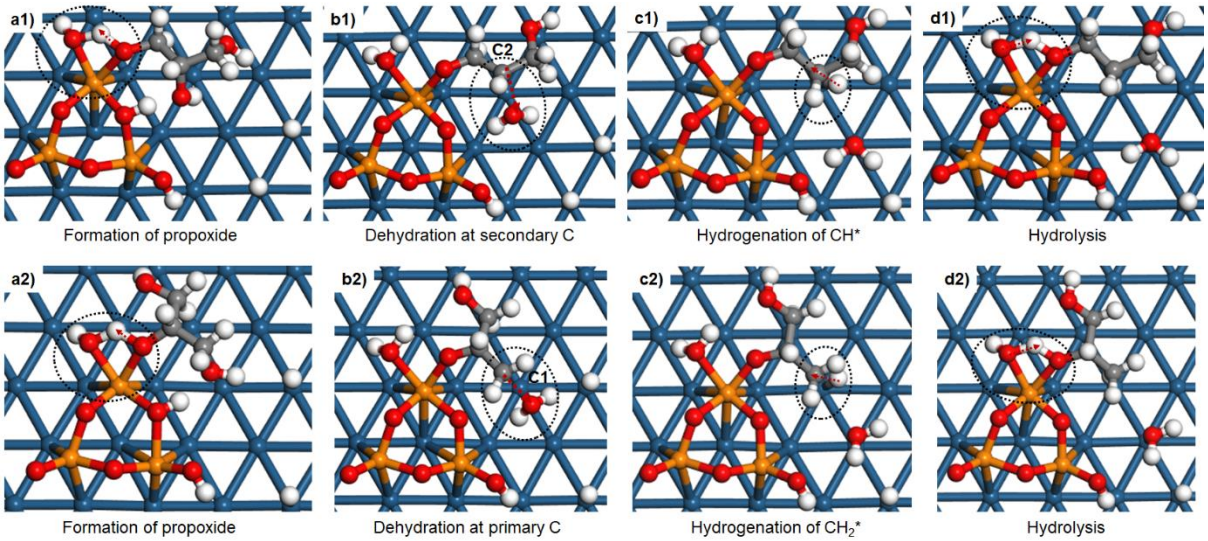

Figure S11 The transition states (TSs) for the hydrogenolysis of glycerol on $Re_3O_6H_3$/Ir(111) catalyst via the protonation-dehydration mechanism as shown in Figure S10. Top panel (a1-d1) shows the hydrogenolysis initiated by the attachment of glycerol as a primary propoxide and bottom panel (a2-d2) shows the hydrogenolysis initiated by the attachment of glycerol as a secondary propoxide. Color code is the same as in Figure 8 of the article.

S3.8. Protonation-dehydration of glycerol by hydronium ion cluster

To investigate the homogeneous acid catalyzed dehydration of glycerol which is attached to the $Re_3O_6H_2$-Ir(111) catalyst as a primary propoxide, a hydrated hydronium ion cluster was used. Here, an $(H_9O_4)^+$ complex with the H_3O^+ ion surrounded by three water molecules, as observed in the *ab initio* molecular dynamics simulation (refer section S2.1. for methodology) was used. This complex was placed suitably next to the glycerol attached to the $Re_3O_6H_2$-Ir(111) catalyst to facilitate hydrogen bonding interaction between the two entities. The optimized structure of this hydronium ion complex interacting with the propoxide is shown in Figure S12a. The water mediated protonation of the secondary hydroxyl of glycerol (as indicated by the black arrows in

Figure S12a) and the elimination of the near neutral OH_2 species (water) as shown in Figure S12b was calculated to have an activation barrier of 200.1 kJ mol^{-1}. The resulting CH* species after the C-O cleavage was adsorbed on the Ir surface as in the case of other C-O cleavage mechanisms described in section 3.4.2 of the article.

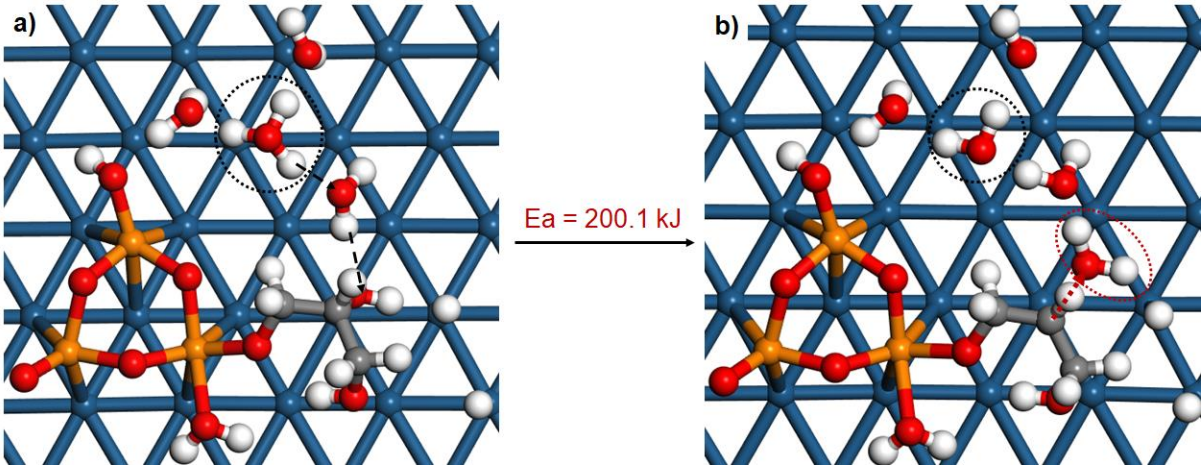

Figure S12 Water mediated protonation-dehydration of glycerol, leading to C-O cleavage at the secondary carbon. **a)** Initial state (IS) showing the hydrated hydronium cluster represented by H_3O^+-$H_2O_{(3)}$ next to the glycerol which is attached to the $Re_3O_6H_2$/Ir(111) catalyst as a primary propoxide. **b)** Transition state (TS) for the protonation dehydration. Color code is the same as in Figure 8 in of the article.

S3.9. Energy profiles and transition states corresponding to formation of propanols on $Re_3O_6H_2$-Ir(111) catalyst

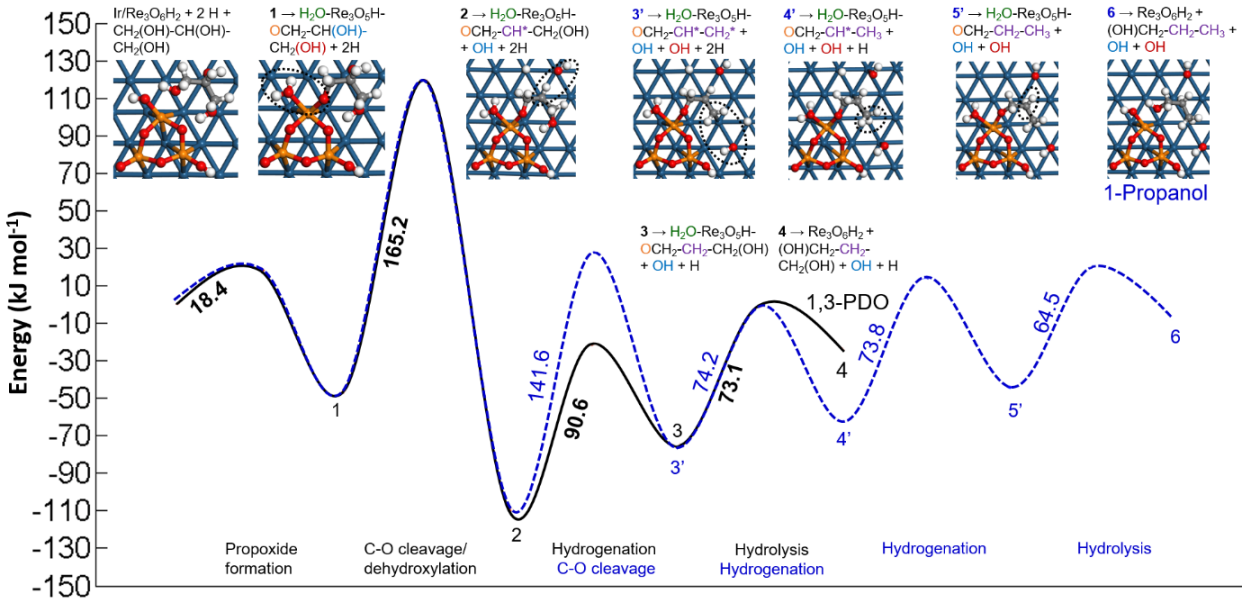

Figure S13 Energy profiles for the formation of 1,3-propanediol (1,3-PDO) (pathway shown in black solid line) and 1-propanol (pathway shown in blue dashed line) from glycerol on the $Re_3O_6H_2$-Ir(111) catalyst. 1-Propanol is formed by the successive elimination of the secondary hydroxyl of glycerol followed by the primary hydroxyl. The activation energy barrier associated with each step is indicated in the figure with representative images and description of the intermediates/product. Color code is the same as in Figure 8 in of the article.

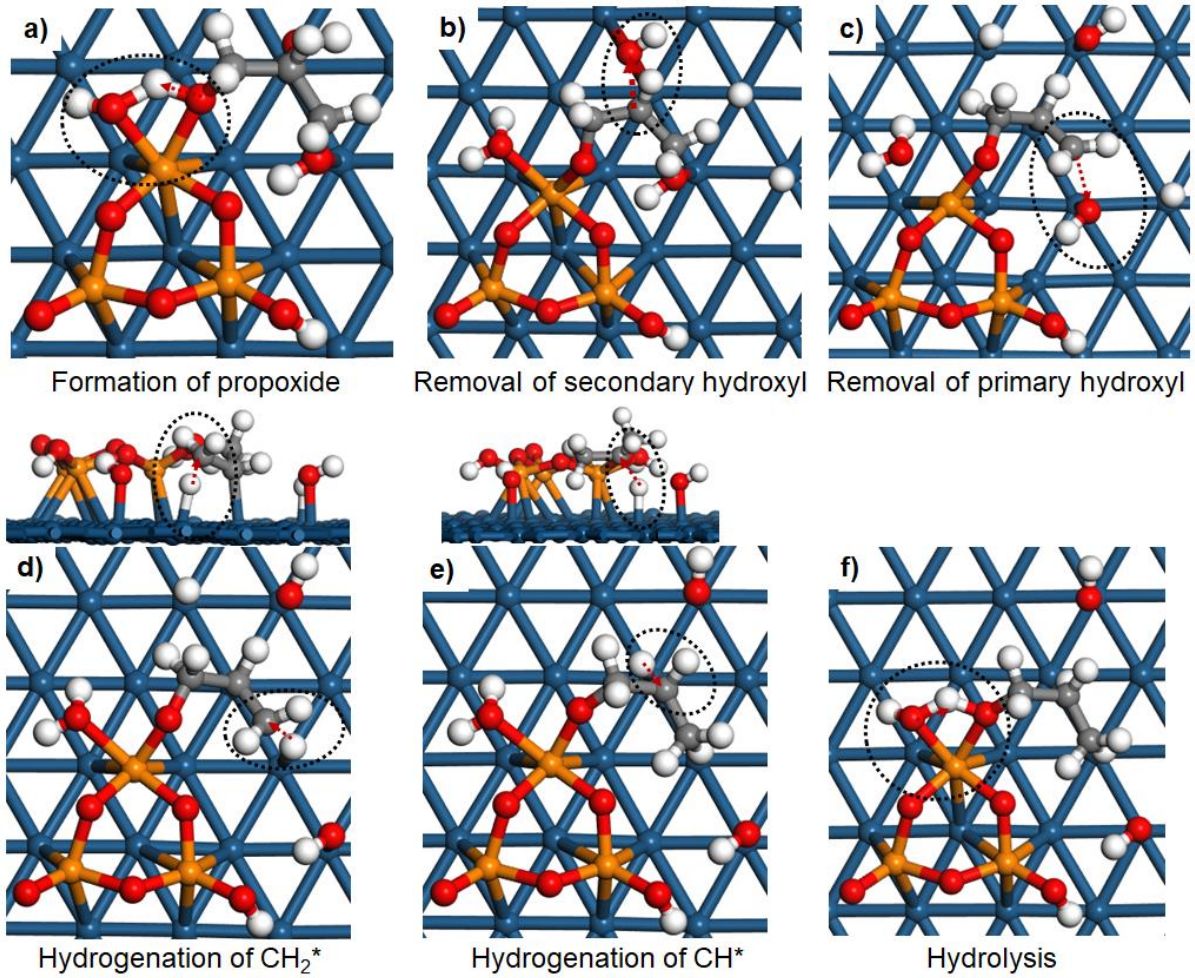

Figure S14 The transition states (TSs) for the successive elimination of hydroxyls of glycerol and direct hydrogenolysis of glycerol on the $Re_3O_6H_2$/Ir(111) catalyst to form 1-propanol as shown in Figure S13. Color code is the same as in Figure 8 in the article.

S3.10. Reactivity of propanediols

Since the C-O bond cleavage or the removal of the hydroxyl is the rate determining step in hydrogenolysis, the reactivity of the propanediols is compared with that of glycerol based on the calculated activation energy barriers for the C-O cleavage step. The transition states for the C-O bond cleavages in propanediols are shown in Figure S15.

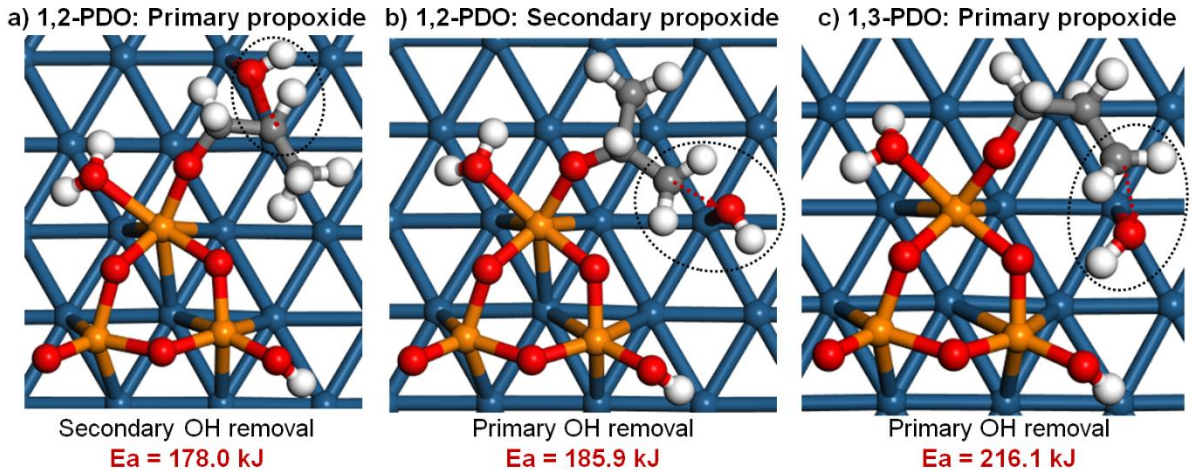

Figure S15 Transition states (TSs) for the C-O cleavage in propanediols on $Re_3O_6H_2$-Ir(111) catalyst, eliminating **a)** the secondary hydroxyl from 1,2-Propanediol (1,2-PDO) when it formed a primary propoxide, **b)** the primary hydroxyl from 1,2-PDO when it formed a secondary propoxide and **c)** the primary hydroxyl from 1,3-Propanediol (1,3-PDO) when it formed a primary propoxide. Activation barriers are also indicated in the figure. Color code is the same as that in Figure 8 of the article.

Table S2. Comparison of reactivity and product selectivity during hydrogenolysis of glycerol and propanediols on ReO_x-Ir catalyst promoted by sulfuric acid.

Substrate	Conversion (%)	Selectivity to (%)			
		1,3-PDO	1,2-PDO	1-PO	2-PO
1,3-PDO	10	--	--	99.0	--
1,2-PDO	83	--	--	85	10
Glycerol	50	35	18	32	10

S3.11. Hydrogenolysis of glycerol on Ir(111) catalysts

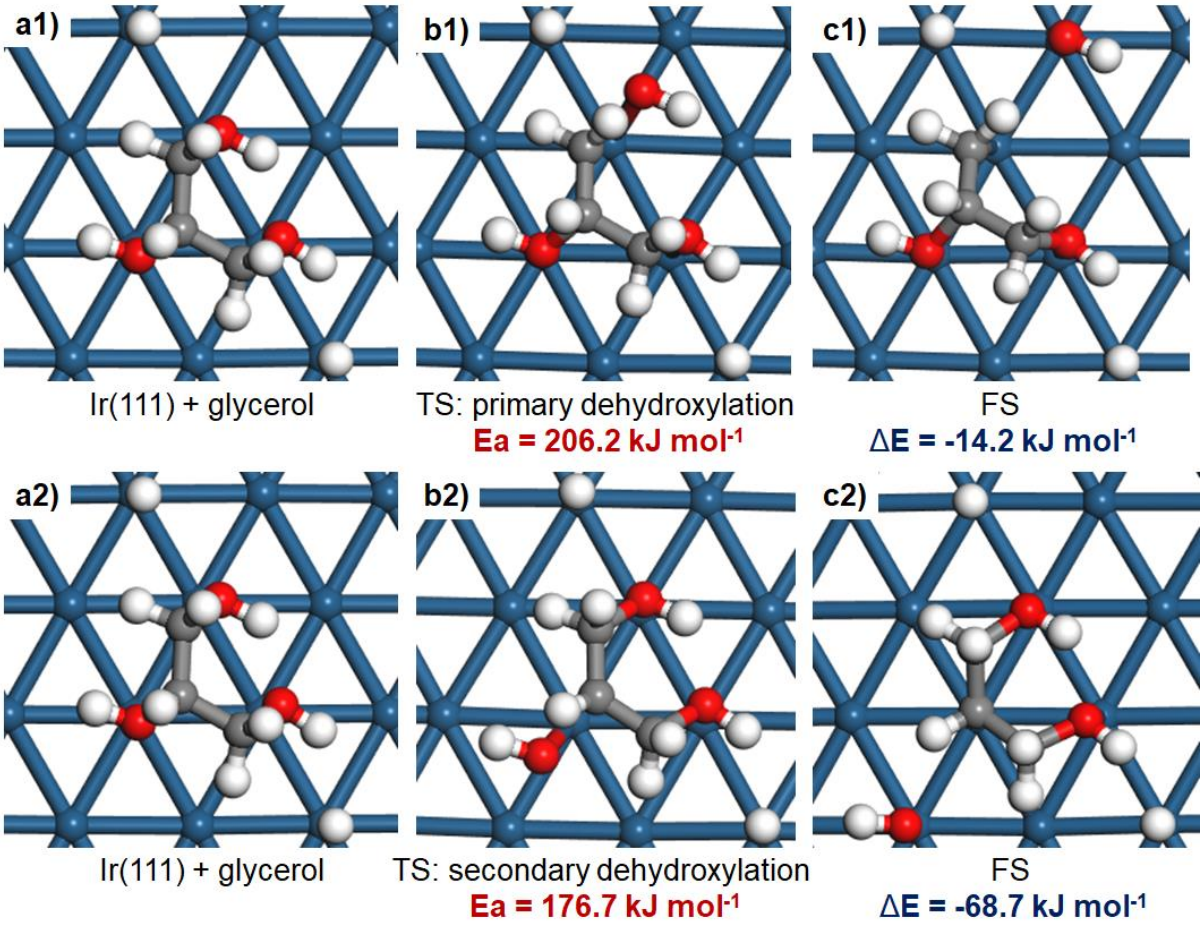

Figure S16 The initial state (IS) of molecularly adsorbed glycerol on the Ir(111) catalyst surface, the transition state (TS) for the direct dehydroxylation, and the final state (FS) of chemisorbed glycerol and OH. Parts a1-c1 show removal of the primary hydroxyl and parts a2-c2 show the removal of the secondary hydroxyl. The activation energy barriers and reaction energies are also indicated. Color code is same as in Figure 8 of the article.

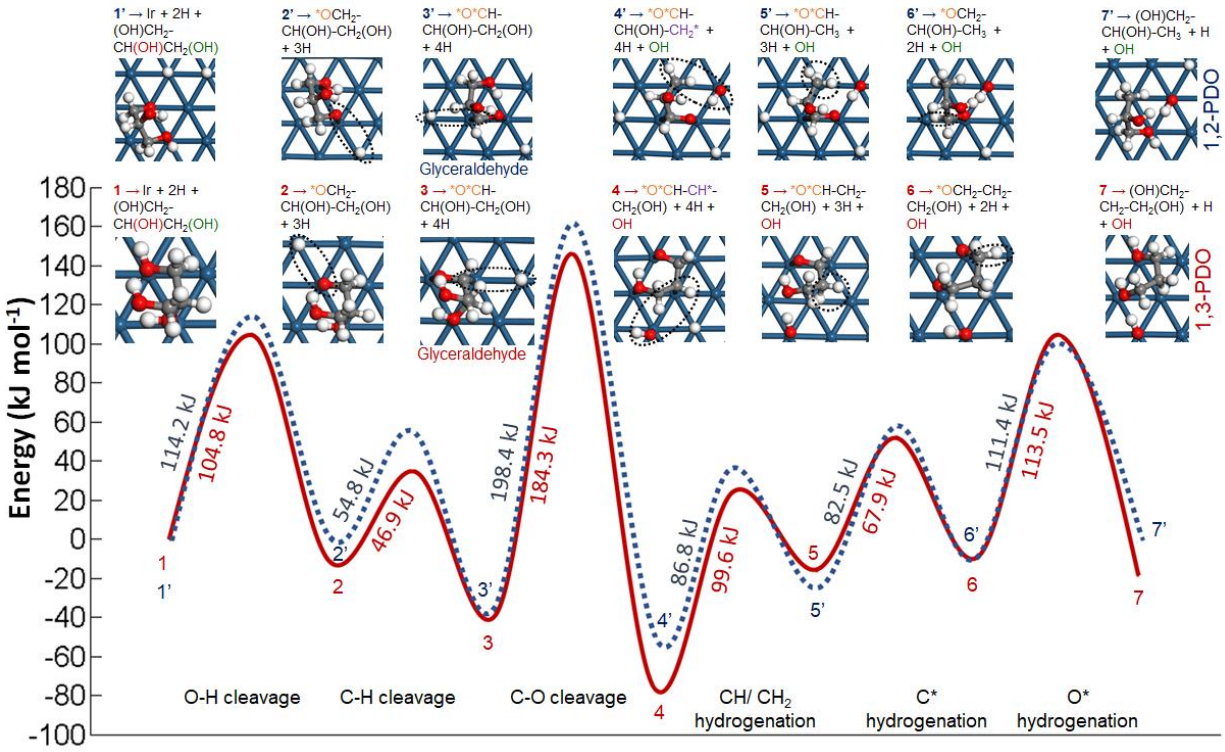

Figure S17 The energy profiles for the hydrogenolysis of glycerol on Ir(111) surface, initiated by the attachment of glycerol through its primary hydroxyl, in a dehydrogenation-dehydroxylation-hydrogenation mechanism, via glyceraldehyde as an intermediate. The profile in blue dotted line represents the removal of the free primary hydroxyl, forming 1,2-PDO, while the profile in red represents the removal of the free secondary hydroxyl, forming 1,3-PDO. The activation energy barrier associated with each step is indicated in the figure with representative images and description of the intermediates/product. Color code is the same as in Figure 8 of the article.

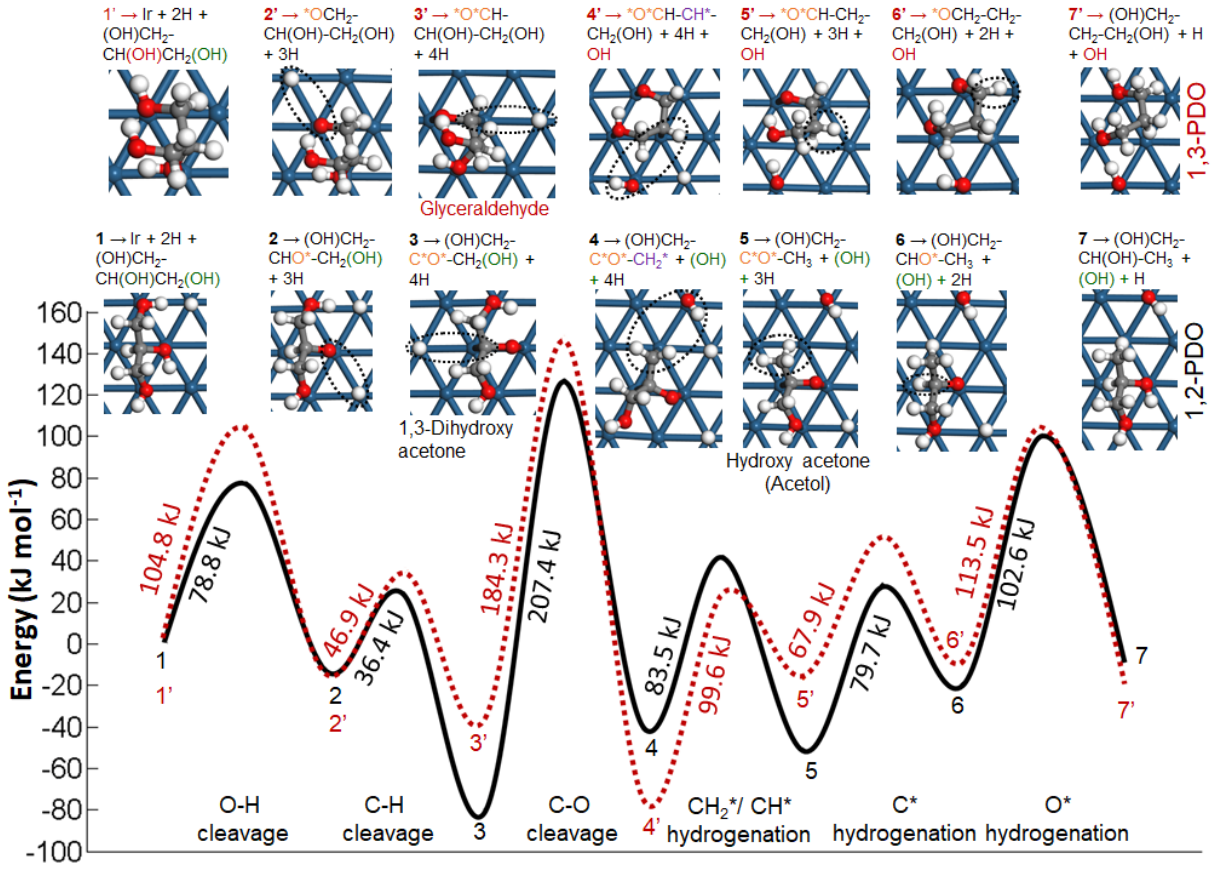

Figure S18 Comparison of the energy profiles for the hydrogenolysis of glycerol on Ir(111) surface initiated by the attachment of glycerol through its primary and secondary hydroxyls, in a dehydrogenation-dehydroxylation-hydrogenation mechanism. The profile in red dotted line represents the removal of the free secondary hydroxyl, forming 1,3-PDO via glyceraldehyde as the intermediate. The profile in black represents the removal of the free primary hydroxyl, forming 1,2-PDO via 1,3-Dihydoxy acetone as an intermediate. The activation energy barrier associated with each step is indicated in the figure with representative images and description of the intermediates/product. Color code is the same as in Figure 8 of the article.

References

1. Car, R.; Parrinello, M., Unified Approach for Molecular Dynamics and Density-Functional Theory, *Phys. Rev. Lett.* **1985,** 55, 2471-2474.

2. *CPMD package,* Version 3.17.1, Copyright IBM Corp 1990-2008, Copyright MPI für Festkörperforschung Stuttgart 1997-2001 (*http://www.cpmd.org/*).

3. Hohenberg, P.; Kohn, W., Inhomogeneous Electron Gas, *Phys. Rev.* **1964,** 136, B864-B871.

4. Kohn, W.; Sham, L. J., Self-Consistent Equations Including Exchange and Correlation Effects, *Phys. Rev.* **1965,** 140, A1133-A1138.

5. Perde w, J. P.; Burke, K.; Ernzerhof, M., Generalized Gradient Approximation Made Simple, *Phys. Rev. Lett.* **1996,** 77, 3865-3868.

6. Troullier, N.; Martins, J. L., Efficient Pseudopotentials for Plane-wave Calculations, *Phys. Rev. B* **1991,** 43, 1993-2006.

7. Nosé, S., A Unified Formulation of the constant Temperature Molecular Dynamics Methods, *J. Chem. Phys.* **1984,** 81, 511-519.

8. Hoover, W. G., Canonical Dynamics: Equilibrium Phase-space Distributions, *Phys. Rev. A* **1985,** 31, 1695-1697.

9. Humphrey, W.; Dalke, A.; Schulten, K., VMD: Visual Molecular Dynamics, *J. Mol. Graph.* **1996,** 14, 33-38.

10. Jorgensen, W. L.; Maxwell, D. S.; Tirado-Rives, J., Development and Testing of the OPLS All-Atom Force Field on Conformational Energetics and Properties of Organic Liquids, *J. Am. Chem. Society* **1996,** 118, 11225-11236.

11. Hess, B., P-LINCS: A Parallel Linear Constraint Solver for Molecular Simulation, *J. Chem. Theory Comput.* **2008,** 4, 116-122.

12. Barzetti, T.; Selli, E.; Moscotti, D.; Forni, L., Pyridine and Ammonia as Probes for FTIR Analysis of Solid Acid Catalysts, *J. Chem. Soc., Faraday Trans.* **1996,** 92, 1401-1407.

13. Falcone, D. D.; Hack, J. H.; Klyushin, A. Y.; Knop-Gericke, A.; Schlögl, R.; Davis, R. J., Evidence for the Bifunctional Nature of Pt-Re Catalysts for Selective Glycerol Hydrogenolysis, *ACS Catal*. **2015,** 5, 5679-5695.

14. Deng, C.; Leng, L.; Zhou, J.; Zhou, X.; Yuan, W., Effects of Pretreatment Temperature on Bimetallic Ir-Re Catalysts for Glycerol Hydrogenolysis, *Cuihua Xuebao/Chinese J. Catal.* **2015,** 36, 1750-1758.

15. Deng, C.; Duan, X.; Zhou, J.; Zhou, X.; Yuan, W.; Scott, S. L., Ir-Re Alloy as a Highly Active Catalyst for the Hydrogenolysis of Glycerol to 1,3-propanediol, *Catal. Sci. Technol.* **2015,** 5, 1540-1547.

16. Castellà-Ventura, M.; Akacem, Y.; Kassab, E., Vibrational Analysis of Pyridine Adsorption on the Brønsted Acid Sites of Zeolites Based on Density Functional Cluster Calculations, *J. Phys. Chem. C* **2008,** 112, 19045-19054.

17. Kresse, G.; Furthmüller, J., Efficient Iterative schemes for Ab Initio Total-Energy Calculations Using a Plane-wave Basis Set. *Phys. Rev. B – Condens. Matter Mater. Phys.* **1996,** *54*, 11169-11186.

18. Luzar, A.; Chandler, D., Effect of Environment on Hydrogen Bond Dynamics in Liquid Water, *Phys. Rev. Lett.* **1996,** 76, 928-931.